Hindawi
Journal of Chemistry
Volume 2023, Article ID 4659034, 9 pages
https://doi.org/10.1155/2023/4659034

Research Article

Extracellular Synthesis of Iron Oxide Nanoparticles Using an Extract of *Bacillus circulans*: Characterization and In Vitro Antioxidant Activity

Ghulam Rabani, Muhammad Dilshad, Aamir Sohail, Aqsa Salman, Saba Ibrahim, Iqra Zafar, and Hafiz Muhammad Arshad

Department of Chemistry, Government College University, Lahore, Pakistan

Correspondence should be addressed to Ghulam Rabani; rabanisaadgcu@gmail.com and Saba Ibrahim; saba_gcu@gcu.edu.pk

Received 16 May 2023; Revised 26 July 2023; Accepted 21 September 2023; Published 16 October 2023

Academic Editor: Ponnurengam Malliappan Sivakumar

This study explores the biosynthesis of iron oxide nanoparticles (IONPs) using *Bacillus circulans* bacterial supernatant as an inexpensive and sustainable alternative to traditional synthesis approaches. The resulting nanoparticles were found to have a uniform size distribution and a spherical shape and agglomerated to form clusters as observed through scanning electron microscopy (SEM). The average diameter of IONPs determined using SEM was 18.37 nm. Characterization using energy-dispersive X-ray spectroscopy (EDX) and X-ray diffraction (XRD) confirmed the synthesis of maghemite (γ-Fe_2O_3) nanoparticles, with a crystallite size of 13.84 nm. Fourier-transform infrared spectroscopy (FT-IR) revealed the surface functional groups of IONPs. Additionally, the IONPs were evaluated for antioxidant activity using the DPPH and ABTS assays, displaying 39.44% inhibition of ABTS radical cations and 35.44% DPPH scavenging. Calcination of IONPs for two hours at 300°C resulted in the conversion to the hematite (α-Fe_2O_3) phase, with a crystallite size of 23.18 nm, and slightly lower antioxidant activity, 35.04% inhibition of ABTS radical cations, and 26.5% DPPH scavenging.

1. Introduction

Nanotechnology is a rapidly evolving area of technology that has recently transformed health, food, agriculture, and industry. Nanotechnology is a vibrant field of science with utile products, including nanorods, nanotubes, and nanoparticles of varying dimensions. It deals with particles of minimal sizes ranging from 1 nm to 100 nm. The nanoparticles possess coveted properties like colloidal stability and optical and magnetic properties, making them a cut above bulk materials [1].

Metal nanoparticles offer promising applications in catalysis, drug delivery, cancer therapy, pollutant removal, water treatment, pigments, cosmetics, and medicine. Scientists have synthesized many metal-based nanoparticles, including silver, gold, zinc, iron, selenium, copper, and chromium nanoparticles. Among these metal nanoparticles, magnetic iron oxide nanoparticles hold prime importance in biomedical applications due to their physiochemical and magnetic properties. The IONPs exist in different polymorphic forms such as α-Fe_2O_3 (hematite), β-Fe_2O_3, γ-Fe_2O_3 (maghemite), FeO (wustite), and Fe_3O_4 (magnetite). Magnetite, hematite, and maghemite are the most prevalent and valuable iron oxide nanoparticles [2]. The separation of a catalyst from the liquid phase can be performed using magnetic IONPs and applying an external magnetic field by small magnets [3]. The magnetic properties of IONPs are beneficial in immobilizing diamagnetic materials such as metal nanoparticles, organocatalysts, and enzymes acting as catalyst support [4]. Moreover, magnetic IONPs are used as contrast agents in MRI and hypothermia treatment [5].

The synthetic pathways are crucial for the properties of the IONPs. The properties of NPs, such as size, crystal

structure, and magnetic and surface properties, are affected mainly by their synthesis route. The synthesis of IONPs is primarily carried by "top-down" and "bottom-up" approaches. The "top-down" techniques involve breaking bulk materials into nanoparticles using physical methods such as sonication, laser ablation, mechanical milling, high-velocity deformation, and physical vapor deposition [6]. These techniques are expensive, time-consuming, and lack the biocompatibility of nanoparticles. The "bottom-up" approaches build nanoparticles from molecular or atomic particles through chemical or biological methods. Several methods to synthesize IONPs rely on chemical processes, which require expensive chemicals and equipment and produce nanoparticles with toxic impurities [7]. The metal-reducing ability of specific metabolites from biological systems such as plants, fungi, and microorganisms inspires biological approaches. Biosynthetic pathways produce nanoparticles using proteins, fatty acids, enzymes, peptides, and flavonoids. The fast growth of microorganisms makes large-scale production of nanoparticles possible [8]. The nanoparticles synthesized using plants or microorganisms are biocompatible, do not contain any toxic impurities, and are safe for medical applications [9]. Moreover, biogenic synthesis reduces energy consumption as all reactions occur at room temperature. Therefore, biological methods to fabricate IONPs are successful tools for producing nanoparticles in an ecofriendly manner.

Microbial synthesis of IONPs has emerged as a cost-effective and sustainable method. Many researchers have used bacteria to fabricate magnetic IONPs with fine control on size, surface, and thermal properties. Bacterial synthesis of IONPs can be carried out intracellular or extracellular. Hassan et al. and Fani et al. reported the extracellular synthesis of IONPs using *E. coli* and *Lactobacillus fermentum,* respectively [10, 11]. Similarly, extracellular synthesis of IONPs by *Bacillus subtilis* and *B. cereus* also has been reported [12, 13]. Mukherjee reported intracellular synthesis of copper, silver, and iron nanoparticles using living cells of *Stenotrphomonas maltophilia* and *Microbacterium marinilacus* [14]. Intracellular synthesis involves binding metal ions or metal oxide ions to the bacteria's cell wall and diffusion into the cell, following the enzymatic reduction into IONPs. In extracellular synthesis, the proteins or enzymes in bacterial extract reduce metal ions into IONPs [15].

However, the bacterial systems produce IONPs much slower, and the incubation period for synthesizing IONPs ranges from 1 day to 10 weeks [16]. Therefore, it is necessary to look for new bacterial strains that can produce nanoparticles more quickly while retaining their critical physiochemical properties. The current study introduces a quick, efficient, and easy strategy for synthesizing IONPs using the supernatant of *Bacillus circulans*. The in vitro antioxidant activity of as-synthesized and calcined IONPs has been measured by DPPH and ABTS assays [17]. IONPs were characterized using UV-visible spectroscopy, FT-IR spectroscopy, FE-SEM, XRD, and EDX [18, 19].

2. Methods

2.1. Growth of Bacterial Cultures. The bacterial colony identified as *Bacillus circulans* was procured from the Department of Zoology microbiology laboratory, Government College University Lahore, Pakistan. The solution of nutrient agar broth in a conical flask containing a loopful of *Bacillus circulans* was incubated overnight at 37°C and 85 rpm in a shaker incubator for maximum growth of bacteria.

2.2. Extraction of Bacterial Supernatant. The bacterial cultures grown overnight were centrifuged at 6000 rpm in 15 ml falcon tubes for 5 minutes. The upper layer of supernatant was isolated into a conical flask. The bacterial pellets were discarded, and the bacterial extract was used to synthesize IONPs.

2.3. Biosynthesis of IONPs. The extracellular biosynthesis of IONPs was carried out by mixing the 25 ml of 0.1 M solutions of $FeSO_4.7H_2O$ and 25 ml bacterial supernatant and shaking the mixture at 80 rpm for five minutes. The mixture containing the bacterial extract and IONPs was centrifuged at 5000 rpm for five minutes to isolate nanoparticles. After washing with distilled water, the nanoparticles were dried in an oven for 24 hours at 60°C and stored to characterize and evaluate the antioxidant activity.

2.4. Optimization of Conditions. The condition optimization for synthesizing IONPs was carried out by changing the concentrations of salt solution, pH, and temperature. The 0.1 M, 0.3 M, 0.5 M, and 1 M salt solutions were used at pH 7 and 40°C. The optimum temperature was found by measuring the yield of IONPs at various temperature conditions of 50°C, 70°C, and 90°C, keeping the concentration of the salt solution and pH constant. Similarly, optimum pH was found by determining the yield of IONPs at various pH values of 5, 6, 7, 8, and 9, keeping concentration and temperature constant.

2.5. Characterization of IONPs. The IONPs were characterized using the UV-visible spectrophotometer, model UV-2300, Techom, with wavelength scanning in the 200–800 nm range; the absorption spectrum associated with surface plasmon resonance of the IONPs was recorded. The surface functional groups and bonds in the IONPs were determined using a Fourier transform infrared (FT-IR) spectrophotometer, IRPrestige-21. The FT-IR spectrum of the bacterial supernatant was recorded to find the potential functional groups responsible for the synthesis of IONPs. The surface roughness and morphology of the IONPs were determined using the FE-SEM (NovaNano SEM 450) at 10kV. The quantitative compositional analysis of the nanoparticles was performed using FE-SEM (NovaNano SEM) with an Oxford EDX detector. An advanced XRD system, Bruker D2-Phaser, was used to identify the crystal structure of the IONPs. The Xpert Highscore Plus was used for peak indexing and phase identification.

2.6. Evaluation of Antioxidant Activity. The antioxidant activity of the IONPs was determined using the ABTS assay and DPPH assay.

2.7. ABTS Assay. ABTS radical cation-based assays are abundant in antioxidant activity tests [20]. In this study, the antioxidant activity of IONPs was evaluated following the modified method of Arnao et al. [21]. 10 μL of 1 mg/ml of IONPs was added to 2.99 ml of $ABTS^{\bullet+}$ solution and kept in the dark for 8 minutes. The absorbance of $ABTS^{\bullet+}$ solution at 734 nm before and after adding NPs solution was recorded using a UV-visible spectrophotometer. The percentage inhibition of $ABTS^{\bullet+}$ was calculated using the following equation:

$$ABTS^{\bullet+}\ \text{Inhibition}\,(\%) = \left(\frac{1-A}{A_0}\right) \times 100, \quad (1)$$

where A_0 is the maximum absorbance of the standard $ABTS^{\bullet+}$ solution and A is the maximum absorbance of the $ABTS^{\bullet+}$ solution following the addition of IONP.

2.8. DPPH Assay. DPPH assay is a hydrogen transfer-based antioxidant activity assay. It is a stable, synthetic radical and is widely used in antioxidant assays. The antioxidant activity of IONPs was determined by DPPH assay following the modified Brand–Williams method. In the DPPH assay, 10 μL of biologically synthesized IONPs was mixed with a 2.5 ml solution of DPPH and shaken vigorously. The maximum absorbance of the DPPH solution at 517 nm and the decrease in absorbance on adding NPs solution were recorded by a UV-visible spectrophotometer. The decrease in absorption of the DPPH solution at 517 nm was recorded. The antioxidant activity was measured by calculating the percentage scavenging of DPPH using the following equation:

$$\text{Percentage DPPH Scavenging} = \left(\frac{1-A}{A_0}\right) \times 100, \quad (2)$$

Here, A and A_0 are the absorbances of the DPPH solution containing IONPs ad standard DPPH solution, respectively.

3. Results and Discussion

3.1. Biosynthesis of IONPs. The IONPs were synthesized extracellularly using a supernatant of *Bacillus circulans*. The yellow color of the bacterial supernatant changed to greenish black immediately after adding a solution of $FeSO_4.7H_2O$, indicating the formation of IONPs. The color change in the appearance of IONPs is due to the surface plasmon resonance of the nanoparticles. The color change is depicted in Figure 1.

The possible mechanism involved in the extracellular synthesis of IONPs using bacterial extract is the bioreduction of Fe^{2+} by proteins in the bacterial supernatant [22]. The first step in this process is the reduction of divalent iron ions (Fe^{2+}) in the precursor salt ($FeSO_4.7H_2O$) to metal form (Fe^0). The proteins in the bacterial supernatant may act as reducing agents. The FT-IR of the bacterial supernatant shows the presence of the –OH group, which is electron-rich and can donate electrons to Fe^{2+}, reducing it to the metal form. The second step encompasses the oxidation of metallic iron atoms to iron oxide. The final step is the stabilization of IONPs by biomolecules in the bacterial supernatant. FT-IR spectrum of as-synthesized IONPs shows the presence of the –OH group on the surface of nanoparticles, showing that it stabilizes IONPs.

3.2. Optimization of Conditions. The yield of IONPs in grams at various temperatures, pH, and concentration conditions was determined. It was observed that maximum IONPs were formed at 40°C and pH 7. At this temperature and pH, the maximum growth of bacteria occurred. The bacterial extract contained maximum biomolecules, and increasing the concentration of salt solution increased the yield. The salt concentration is directly related to the yield of IONPs because of increasing metal ions (Figure 2(a)). The bacteria showed no growth at pH 5, and at pH 6, the yield was low. The highly acidic or basic conditions retard the growth of bacteria which in turn produce little metabolites, and the yield of nanoparticles also decreases (Figure 2(c)). The effect of temperature had a variable effect showing a maximum yield at 40°C and then a decrease in yield at 50°C. The reaction speed was more significant at higher temperatures, and an intense color change was observed; however, the yield was low. The decrease in yield at 50°C and then increase up to 70°C indicates the presence of more than one metabolite in bacterial extract responsible for producing nanoparticles. Some metabolites could not tolerate temperatures higher than 40°C and start denaturing. The other metabolites tolerated temperatures even higher than 50°C and the yield of IONPs increased. At 90°C, all the metabolites start denaturing, and the yield of nanoparticles drops (Figure 2(b)).

3.3. Characterization of IONPs. The fabrication of IONPs was further evaluated using various characterization techniques such as UV-visible spectroscopy, FTIR spectroscopy, FE-SEM, EDX, and XRD. The UV-visible scan of the 5% diluted solution of nanoparticles was performed in the 200–800 nm range.

3.4. UV-Visible Spectroscopic Analysis. The UV-visible spectrum of the as-synthesized IONPs shows maximum absorption at 225 nm within the surface plasmon resonance range of the IONPs (Figure 3). The very intense peak depicts the fabrication of many small-sized IONPs. The peak in the UV-visible spectrum corresponds to the surface plasmon resonance (SPR) of maghemite (γ-Fe_2O_3) NPs. Chauhan and Upadhyay have reported similar absorption by iron oxide nanoparticles produced using an extract of *Lawsonia inermis*. They observed an absorption peak around 224 nm [23]. The optical band gap of as-synthesized IONPs calculated using a Tauc plot is 5.39 eV (Figure 4). The higher value of the band gap indicates small-sized nanoparticles. Small nanoparticles have fewer atoms and poor orbital overlap, increasing the band gap.

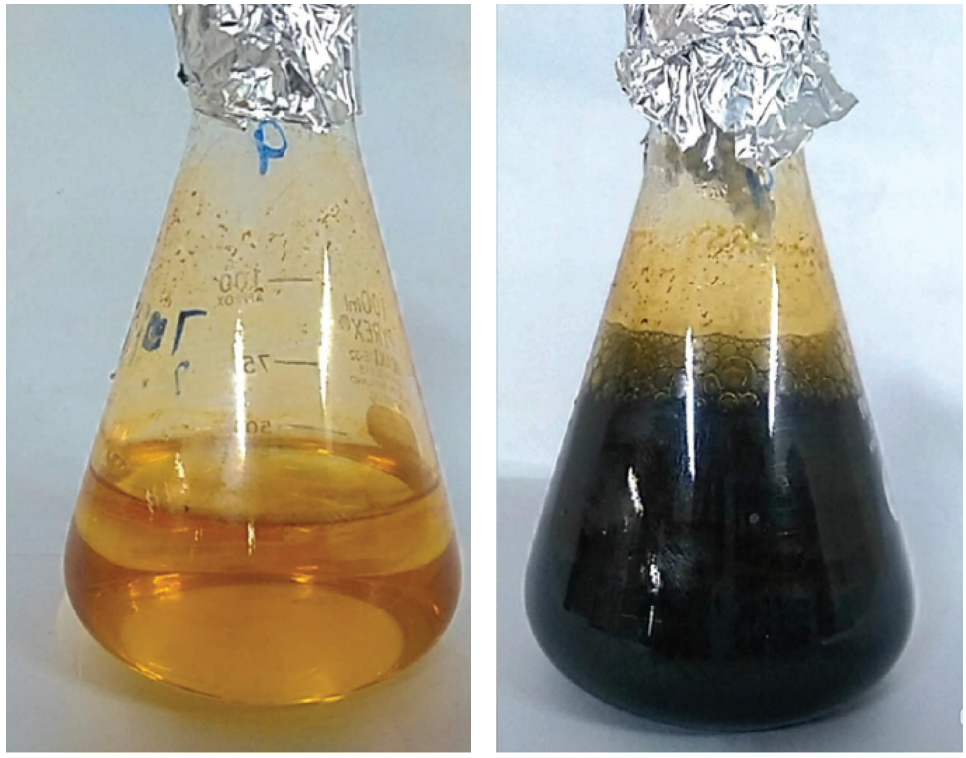

(a) (b)

Figure 1: (a) Bacterial supernatant and (b) color change on formation of IONPs.

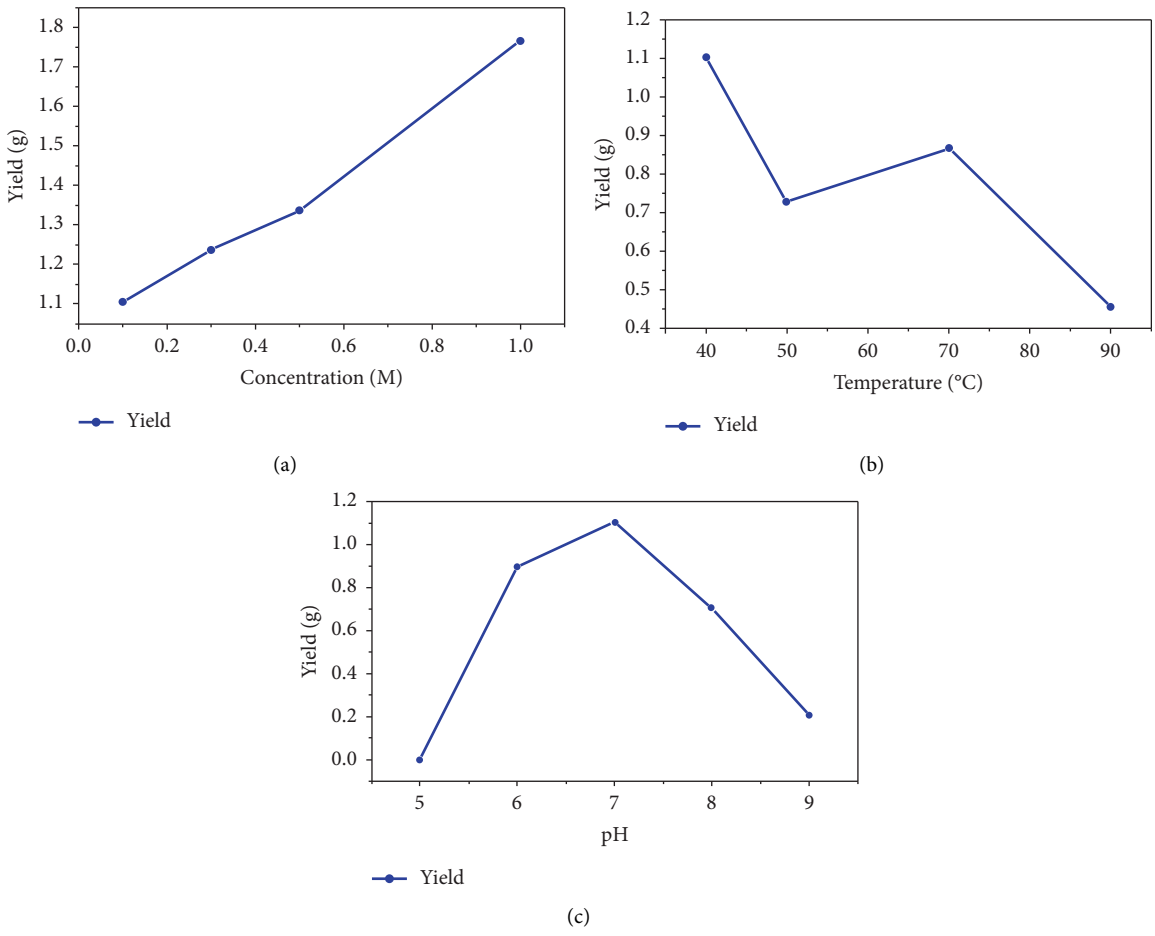

Figure 2: Optimization of conditions: (a) effect of concentration, (b) effect of temperature, and (c) effect of pH.

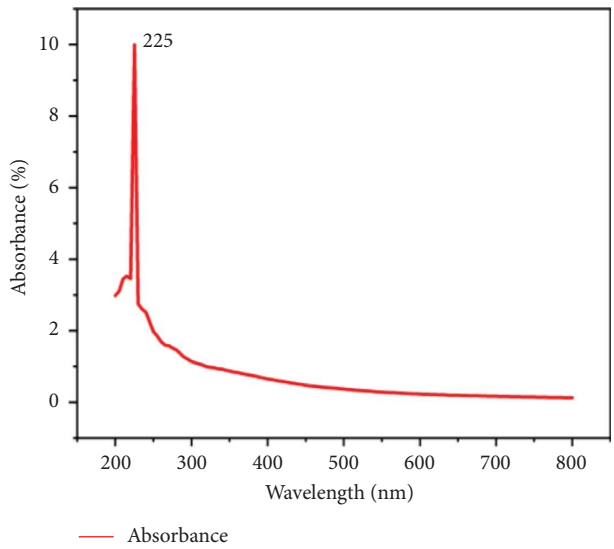

Figure 3: UV-visible spectrum of IONPs synthesized in this study.

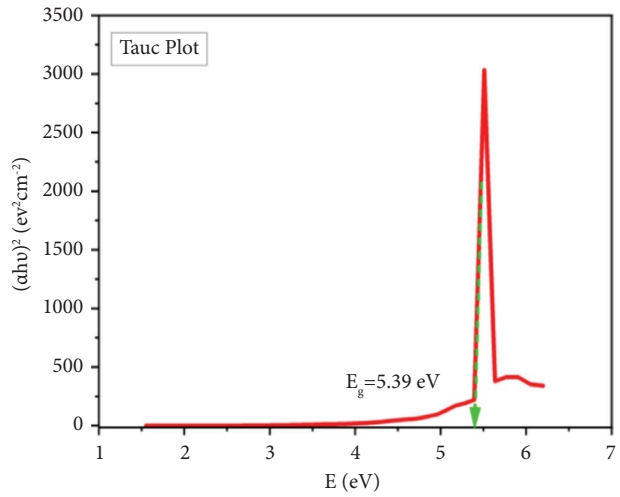

Figure 4: Direct Tauc plot for band gap of IONPs.

3.5. FT-IR Spectroscopic Analysis. FT-IR analysis of bacterial supernatants was used to recognize the functional groups responsible for synthesizing iron oxide nanoparticles (IONPs). The surface functional groups on IONPs were also identified using FT-IR (Figure 5(b)). The broad peak at 3303 cm^{-1} in the spectrum of the bacterial supernatant corresponds to the stretching of the C-H group of carboxylic acid, indicating the presence of specific proteins or fatty acids in the bacterial supernatant involved in the synthesis of IONPs. In addition, the peaks at 1569 cm^{-1} and 1400 cm^{-1} correspond to the stretch vibrations of the C=O and C-O groups. The peak at 1086 cm^{-1} corresponds to the bending of C-H bonds. According to a correlation analysis by Lozano et al. the fatty acids show bands around 2925, 2854, and 1746 cm^{-1}, whereas proteins show bands around 3288, 1657, and 1542 cm^{-1} [24]. From this correlation analysis, it can be inferred that the biomolecules present in the bacterial supernatant in the current study are proteins.

FT-IR spectrum of the as-synthesized IONPs reveals the presence of surface O-H groups as indicated by a peak at 3244 cm^{-1}. Additionally, the peak at 995 cm^{-1} corresponds to C-H bending, indicating the presence of biomolecules acting as capping agents to stabilize the IONPs. The peak at 472 cm^{-1} corresponds to Fe-O stretching vibrations, characteristic of IONPs. Finally, the 1632 cm^{-1} and 1431 cm^{-1} peaks correspond to C=O and C-O stretching vibrations, respectively (Figure 5(a)). The peaks corresponding to C-H bending and C=O and C-O stretching vibrations confirm that the biomolecules act as capping agents and stabilize the IONPs. The surface of IONPs is covered with biomolecules such as amino acids or peptides.

3.6. SEM Analysis. The SEM analysis of morphological features revealed the spherical, uniform, and granular morphology of the as-synthesized IONPs. The nanoparticles were agglomerated, forming irregularly shaped clusters. The cluster formed due to the capping agents covering the nanoparticles' surface. The mean diameter of IONPs determined using SEM was 18.34 nm. The SEM images highlighted the surface roughness of as-synthesized IONPs (Figure 6). Figure 7 shows the uniform size distribution of the nanoparticles.

3.7. EDX Analysis. The EDX analysis revealed the elemental composition of as-synthesized IONPs. The EDX spectrum indicates that the IONPs primarily comprise Fe, O, and C. Fe, O, and C percentages are 41.74%, 27.36%, and 11.39%, respectively (Table 1). It is inferred from the relative weight percentage of Fe and O that IONPs are chemically Fe_2O_3. The C signal in the spectrum indicates the presence of biomolecules stabilizing the nanoparticles (Figure 8).

3.8. XRD Analysis. The X-ray diffraction (XRD) pattern revealed that the as-synthesized iron oxide nanoparticles (IONPs) comprised two phases. The peaks at 76.44°, 75.44°, 50.086°, 35.62°, and 18.35° are indexed to (630), (622), (421), (311), and (111), respectively (Figure 9). The relative intensities and positions of these peaks closely matched the maghemite crystal structure (γ-Fe_2O_3) corresponding to ICCD card number 39–1346, confirming that the major phase of the IONPs is the cubic crystalline form of maghemite (γ-Fe_2O_3). Additionally, the peaks positioned at 45.38°, 31.66°, and 28.64° are indexed to (160), (102), and (230), respectively, and closely matched the miller indices given in ICCD card no. 33–0665 confirms the presence of the orthorhombic crystalline phase of iron oxide carbonate. The peaks other than IONPs appear due to the presence of biomolecules contributing to the production of iron oxide carbonate. The as-synthesized IONPs had an average crystallite size of 13.84 nm, which was calculated using the following equation:

$$D = \frac{K\lambda}{B\,\mathrm{Cos}\,\theta}, \tag{3}$$

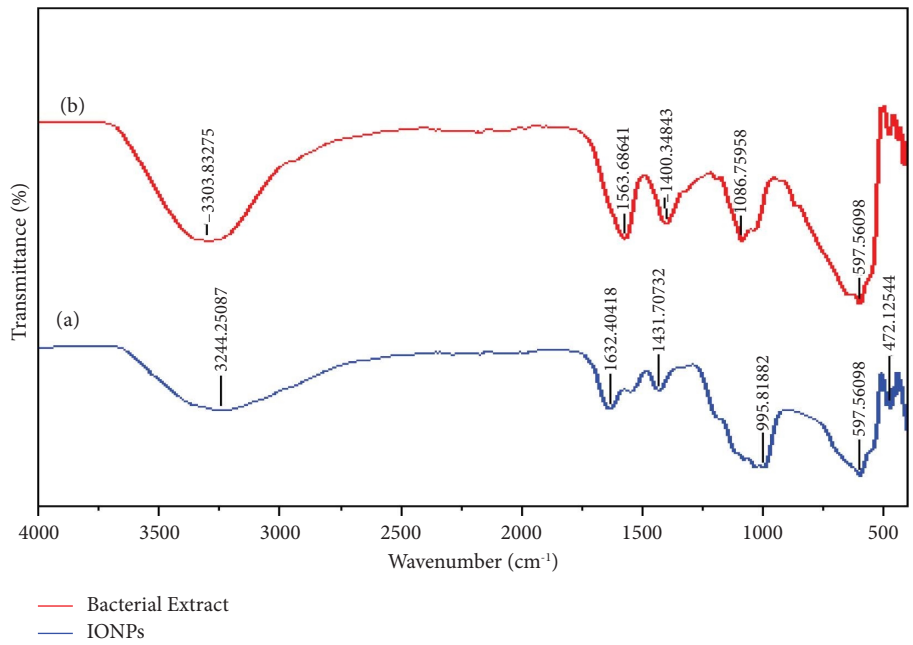

Figure 5: FT-IR spectrum of (a) IONPs synthesized in this study (b) Bacterial supernatant.

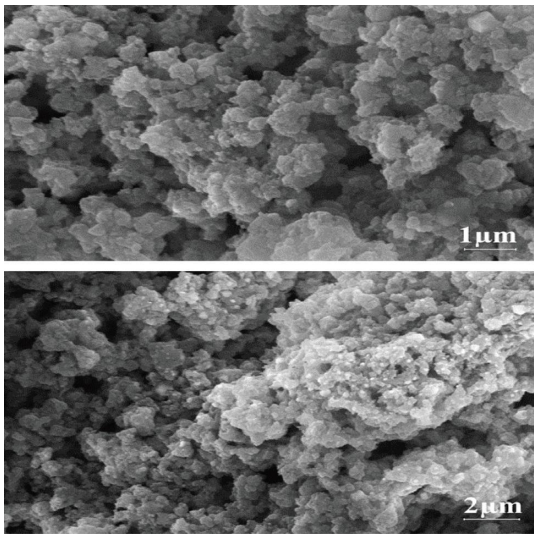

Figure 6: SEM image of as-synthesized IONPs.

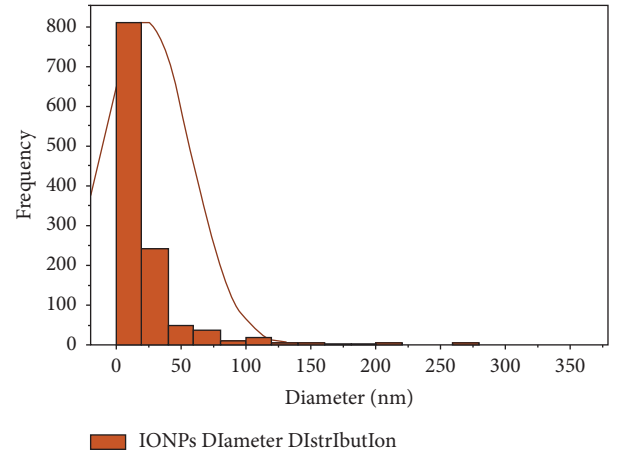

Figure 7: Size distribution curve of IONPs.

where D = crystallite size, K = Scherrer constant, B = FWHM values of the peaks, λ = X-ray wavelength, and θ = Bragg's angle.

The phase identification of the calcined IONPs was performed using an XRD pattern. The peak analysis revealed that the calcined IONPs have hematite and iron oxide carbonate phases. The diffraction peaks positioned at 75.47°, 54.087°, 49.625°, 35.903°, 33.37°, and 24.5° are indexed to (220), (116), (024), (110), (104), and (012), respectively (Figure 10). These peaks are closely related to the peak position and intensities of rhombohedral hematite (α-Fe_2O_3) corresponding to ICCD card number 33–0664.

Table 1: Elemental composition of as-synthesized IONPs.

Elements	Weight %
C	11.39
O	41.74
Fe	27.36
S	5.8
Cl	5.9

The peaks at 45.75°and 31.89° indexed to (160) and (102), respectively, closely matched the peaks of the orthorhombic crystalline phase of iron oxide carbonate according to ICCD card number 33–0665. The average crystallite size of calcined IONPs calculated using the Scherrer equation was 23.18 nm.

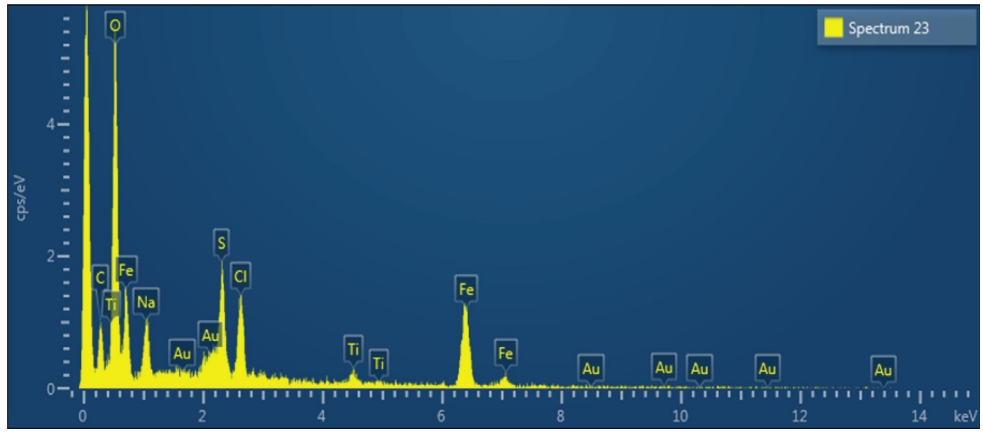

Figure 8: EDX elemental map of IONPs.

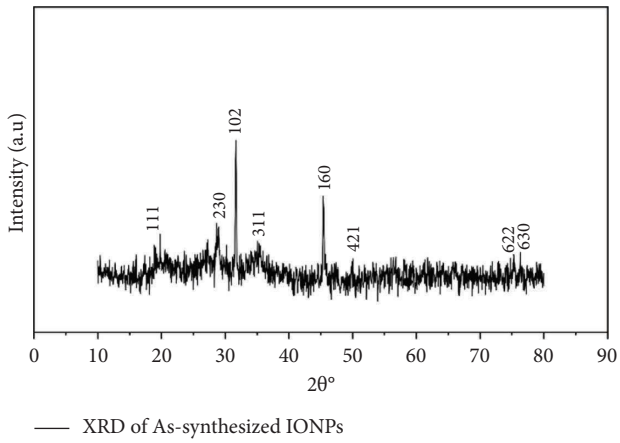

Figure 9: XRD pattern of as-synthesized IONPs.

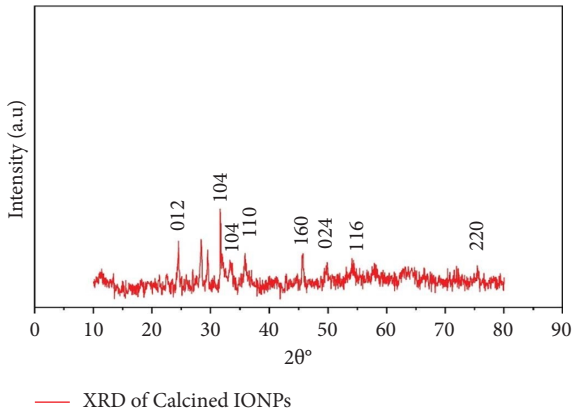

Figure 10: XRD pattern of calcined IONPs.

3.9. In Vitro Antioxidant Activity

3.9.1. ABTS Assay. The extent of decoloration of the blue-green solution of $ABTS^{\bullet+}$ is a measure of the antioxidant activity of the IONPs [25, 26]. The in vitro antioxidant activity by ABTS assay showed the higher antioxidant activity of as-synthesized IONPs than the calcined IONPs. The antioxidant activity of as-synthesized and calcined IONPs was expressed as percentage inhibition of $ABTS^{\bullet+}$. As-synthesized IONPs with 39.44% of percentage $ABTS^{\bullet+}$ inhibition were more effective antioxidants than calcined IONPs with 35.04% of percentage $ABTS^{\bullet+}$ inhibition. DPPH Assay: The DPPH is a stable, synthetic radical widely used in antioxidant activity assays. The color of the DPPH radical solution is deep purple and fades away upon adding IONPs. The percentage of DPPH scavenging measures the antioxidant activity of the nanoparticles. The DPPH assay of the IONPs synthesized in this study revealed that as-synthesized IONPs are more significant antioxidants with a percentage DPPH scavenging of 35.44% compared to calcined IONPs having a percentage DPPH scavenging of 26.5%. The enhanced antioxidant activity of as-synthesized IONPs compared to bare IONPs is because of biomolecules on the surface of nanoparticles that act as effective hydrogen sources. The DPPH scavenging activity of both the as-synthesized and calcined IONPs was less than $ABTS^{\bullet+}$ inhibition activity, possibly due to different mechanisms involved in the free radical scavenging. The results are shown in Figure 11.

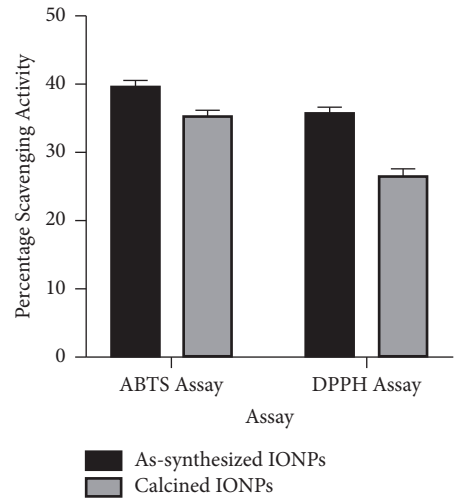

Figure 11: Comparison of the antioxidant activity of as-synthesized and calcined IONPs.

The higher antioxidant activity of as-synthesized IONPs than calcined IONPs is due to the presence of biomolecules covering the surface. The surface of as-synthesized IONPs is covered with biomolecules rich in hydrogen and electrons which are responsible for higher antioxidant activities by hydrogen transfer or electron transfer mechanisms. During calcination, the biomolecules on the surface of NPs decomposed and the antioxidant activity of calcined IONPs decreased.

4. Conclusion

The iron oxide nanoparticles (IONPs) were produced using *Bacillus circulans* supernatant and were found to be spherical with a mean diameter of 18.32 nm and were agglomerated, forming irregular-shaped clusters. The nanoparticles were analyzed using various techniques such as UV-visible spectroscopy, FT-IR spectroscopy, SEM, EDX, and XRD. The majority of the as-synthesized IONPs were found to be maghemite (γ-Fe_2O_3), while the calcined IONPs were primarily hematite (α-Fe_2O_3). The optical band gap of IONPs was found to be 5.39 ev showing the formation of ultrasmall nanoparticles. The as-synthesized IONPs have shown more significant ABTS radical cation inhibition and DPPH scavenging activity than calcined IONPs. Their use can be extended to degrading dyes and removing heavy metals from wastewater.

Data Availability

The data used to support the study are available in the paper.

Disclosure

Ghulam Rabani and Muhammad Dilshad are the co-first authors.

Conflicts of Interest

The authors declare that there are no conflicts of interest.

Authors' Contributions

Ghulam Rabani and Muhammad Dilshad were involved in research design, experimentation, analysis of results, and writeup. They have been also involved in study conception and manuscript preparation. *Saba Ibrahim* helped in the analysis of results and writeup. She has been also involved to design the research and literature survey. *Aqsa Salman and Aamir Sohail* helped in the literature survey and writeup. They also helped in interpretation of various spectra and formatting. *Iqra Zafar and Muhammad Arshad* did the final review of language editing and formatting. They also did formal analysis of the results. *Ghulam Rabani* and *Muhammad Dilshad* contributed equally to this work.

References

[1] F. Batool, M. S. Iqbal, S.-U.-D. Khan, J. Khan, B. Ahmed, and M. I. J. S. R. Qadir, "Biologically synthesized iron nanoparticles (FeNPs) from Phoenix dactylifera have anti-bacterial activities," *Scientific Reports*, vol. 11, pp. 22132–22139, 2021.

[2] W. Wu, Z. Wu, T. Yu, C. Jiang, and W. S. J. S. Kim, "Amp; materials, t.o.a," *Recent progress on magnetic iron oxide nanoparticles: synthesis, surface functional strategies and biomedical applications*, vol. 16, 2015.

[3] L. M. Rossi, N. J. Costa, F. P. Silva, and R. J. G. C. Wojcieszak, "Magnetic nanomaterials in catalysis: advanced catalysts for magnetic separation and beyond," *Green Chemistry*, vol. 16, pp. 2906–2933, 2014.

[4] M. Jacinto, M. Gonzales, A. Zanato, J. Gil, and D. J. S. C. Souza, "Rh nanoparticles grafted on mesoporous silica support as a high-efficiency catalyst for Anthracene hydrogenation," *Sustainable Chemistry and Pharmacy*, vol. 6, pp. 90–95, 2017.

[5] S. Laurent, S. Dutz, U. O. Häfeli, M. J. A. Mahmoudi, and I. science, "Magnetic fluid hyperthermia: focus on superparamagnetic iron oxide nanoparticles," *Advances in Colloid and Interface Science*, vol. 166, no. 1-2, pp. 8–23, 2011.

[6] V. Arole and S. J. J. M. S. Munde, "Fabrication of nanomaterials by top-down and bottom-up approaches-an overview," *JAAST:Material Science*, vol. 1, pp. 89–93, 2014.

[7] P. Torabian, F. Ghandehari, and M. J. A. J. O.G. C. Fatemi, "Biosynthesis of iron oxide nanoparticles by cytoplasmic extracts of bacteria lactobacillus casei," *Asian Journal of Green Chemistry*, vol. 2, pp. 181–188, 2018.

[8] T. J. Park, K. G. Lee, and S. Y. Lee, "Advances in microbial biosynthesis of metal nanoparticles," *Applied Microbiology and Biotechnology*, vol. 100, no. 2, pp. 521–534, 2016.

[9] R. Augustine and A. Hasan, "Emerging applications of biocompatible phytosynthesized metal/metal oxide nanoparticles in healthcare," *Journal of Drug Delivery Science and Technology*, vol. 56, Article ID 101516, 2020.

[10] D. F. Hassan and M. Mahmood, "Biosynthesis of iron oxide nanoparticles using Escherichia coli," *Iraqi Journal of Science*, vol. 66, pp. 453–459, 2019.

[11] M. Fani, F. Ghandehari, and M. J. J. M. C. S. Rezaee, "Biosynthesis of iron oxide nanoparticles by cytoplasmic extract of bacteria lactobacillus fermentum," *Asian Journal of Green Chemistry*, vol. 1, pp. 28–30, 2018.

[12] P. A. Sundaram, R. Augustine, and M. Kannan, "Extracellular biosynthesis of iron oxide nanoparticles by Bacillus subtilis strains isolated from rhizosphere soil," *Biotechnology and Bioprocess Engineering*, vol. 17, no. 4, pp. 835–840, 2012.

[13] M. Fatemi, N. Mollania, M. Momeni-Moghaddam, and F. Sadeghifar, "Extracellular biosynthesis of magnetic iron oxide nanoparticles by Bacillus cereus strain HMH1: characterization and in vitro cytotoxicity analysis on MCF-7 and 3T3 cell lines," *Journal of Biotechnology*, vol. 270, pp. 1–11, 2018.

[14] P. Mukherjee, "Stenotrophomonas and Microbacterium: mediated biogenesis of copper, silver and iron nanoparticles—proteomic insights and antibacterial properties versus biofilm formation," *Journal of Cluster Science*, vol. 28, no. 1, pp. 331–358, 2017.

[15] P. Singh, Y.-J. Kim, D. Zhang, and D. C. Yang, "Biological synthesis of nanoparticles from plants and microorganisms," *Trends in Biotechnology*, vol. 34, no. 7, pp. 588–599, 2016.

[16] V. Chmykhalo, A. Belanova, M. Belousova et al., "Microbial-based magnetic nanoparticles production: a mini-review," *Integrative Biology*, vol. 13, no. 4, pp. 98–107, 2021.

[17] S. Majeed, M. Danish, M. N. Mohamad Ibrahim et al., "Bacteria mediated synthesis of iron oxide nanoparticles and their antibacterial, antioxidant, cytocompatibility properties," *Journal of Cluster Science*, vol. 32, no. 4, pp. 1083–1094, 2021.

[18] S. A. M. K. Ansari, E. Ficiarà, F. A. Ruffinatti et al., "Magnetic iron oxide nanoparticles: synthesis, characterization and functionalization for biomedical applications in the central nervous system," *Materials*, vol. 12, no. 3, p. 465, 2019.

[19] M. Salehiabar, H. Nosrati, S. Davaran, H. Danafar, and H. K. J. D. R. Manjili, "Facile synthesis and characterization of L-aspartic acid coated iron oxide magnetic nanoparticles (IONPs) for biomedical applications," *Drug Research*, vol. 68, no. 05, pp. 280–285, 2018.

[20] K. Thaipong, U. Boonprakob, K. Crosby, L. Cisneros-Zevallos, and D. Byrne, "Analysis Comparison of ABTS, DPPH, FRAP, and ORAC assays for estimating antioxidant activity from guava fruit extracts," *Journal of Food Composition and Analysis*, vol. 19, pp. 669–675, 2006.

[21] M. B. Arnao, A. Cano, and M. J. F. C. Acosta, "The hydrophilic and lipophilic contribution to total antioxidant activity," *Food Chemistry*, vol. 73, pp. 239–244, 2001.

[22] S. A. Akintelu, A. K. Oyebamiji, S. C. Olugbeko, and A. S. Folorunso, "Green synthesis of iron oxide nanoparticles for biomedical application and environmental remediation: a review," *Eclética Química*, vol. 46, pp. 17–37, 2021.

[23] S. Chauhan and L. S. B. Upadhyay, "Biosynthesis of iron oxide nanoparticles using plant derivatives of Lawsonia inermis (Henna) and its surface modification for biomedical application," *Nanotechnology for Environmental Engineering*, vol. 4, no. 1, p. 8, 2019.

[24] M. Lozano, P. Rodriguez-Ulibarri, J. Echeverría, M. Beruete, M. Sorolla, and M. J. Beriain, "Mid-infrared spectroscopy (MIR) for simultaneous determination of fat and protein content in meat of several animal species," *Food Analytical Methods*, vol. 10, pp. 3462–3470, 2017.

[25] I. R. Ilyasov, V. L. Beloborodov, I. A. Selivanova, and R. P. J. I. J. O.M. S. Terekhov, "ABTS/PP decolorization assay of antioxidant capacity reaction pathways," *International Journal of Molecular Sciences*, vol. 21, no. 3, p. 1131, 2020.

[26] K. Kut, B. Cieniek, I. Stefaniuk, G. Bartosz, and I. J. P. Sadowska-Bartosz, "A modification of the ABTS• decolorization method and an insight into its mechanism," *Processes*, vol. 10, no. 7, p. 1288, 2022.

[27] M. Szabo, C. Idiţoiu, D. Chambre, and A. J. C. P. Lupea, "Improved DPPH determination for antioxidant activity spectrophotometric assay," *Chemical Papers*, vol. 61, no. 3, pp. 214–216, 2007.

[28] W. Brand-Williams, M. E. Cuvelier, and C. J. L. F. S. Berset, "Technology use of a free radical method to evaluate antioxidant activity," *LWT- Food Science and Technology*, vol. 28, no. 1, pp. 25–30, 1995.

[29] J. Iqbal, B. A. Abbasi, R. Ahmad et al., "Biogenic synthesis of green and cost effective iron nanoparticles and evaluation of their potential biomedical properties," *Journal of Molecular Structure*, vol. 1199, Article ID 126979, 2020.

[30] H. Nosrati, M. Salehiabar, S. Davaran, A. Ramazani, H. K. Manjili, and H. J. R. Danafar, "New advances strategies for surface functionalization of iron oxide magnetic nano particles (IONPs)," *Research on Chemical Intermediates*, vol. 43, no. 12, pp. 7423–7442, 2017.